ACS APPLIED MATERIALS & INTERFACES

Research Article

www.acsami.org

Facile One-Pot Synthesis of Highly Porous Carbon Foams for High-Performance Supercapacitors Using Template-Free Direct Pyrolysis

Chengwei Wang, Michael J. O'Connell, and Candace K. Chan*

Materials Science and Engineering School for Engineering of Matter, Transport and Energy, Arizona State University, Tempe, Arizona 85287, United States

Supporting Information

ABSTRACT: Foam-like porous carbons with specific surface area (SSA) up to 2340 m^2/g were synthesized using direct pyrolysis of sugar and zinc nitrate mixtures without any hard templates. The role of the ZnO nanoparticles formed from the decomposition of zinc nitrate, and the effects of high-temperature annealing on the formation of the high-SSA carbon foams were systematically studied. Due to the facile and quick reaction conditions, these carbon foams could be easily synthesized on a large scale. When used as supercapacitor electrode materials, a specific capacitance up to 280 F/g was achieved at current density of 0.1 A/g and remained as high as 207 F/g, even at a high current density of 10 A/g.

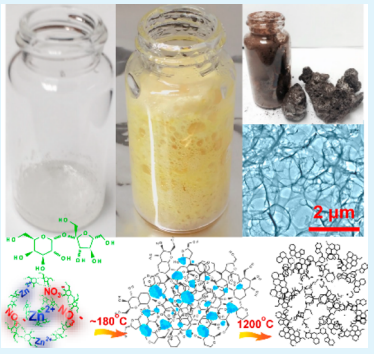

KEYWORDS: *porous, carbon, ZnO, supercapacitor, electrochemical capacitor*

1. INTRODUCTION

Highly porous carbon foams have attracted much attention recently for use in several applications as low-cost materials with ultrahigh specific surface area (SSA) and facile synthesis, especially for energy storage devices such as supercapacitors[1,2] and batteries.[3] Unlike carbon nanotubes or graphene, which require strict chemical vapor deposition (CVD)[4−7] conditions or complicated chemical exfoliation processes,[8,9] carbon foam can be synthesized in large quantities simply by direct pyrolysis of carbon precursors such as polymers[10−12] or sugars.[2,3,13] Using direct pyrolysis of sugar in the presence of inorganic catalysts, the SSA of carbon foams is usually below 1000 m^2/g.[2,13,14] However, with further activation, the SSA can reach as high as 1500−3000 m^2/g.[3,14] For example, Wang et al.[2] used the decomposition of ammonium salt to generate gas bubbles, which created a blowing effect on melted sugar to form carbon with a strutted graphene structure and SSA of 1005 m^2/g. However, this reaction needed to be done at a relatively slow heating rate (4 °C/min), making it time-consuming. By using ZnO nanoparticles as template and etchant at high temperature, Strubel et al.[3] synthesized porous carbon foam with SSA up to 3060 m^2/g, which demonstrated very impressive performance as an electrode in a lithium−sulfur battery. Three-dimensional aperiodic hierarchical porous carbon was also synthesized by carbonization of resin with $Ni(OH)_2$ as catalyst.[15] However, these techniques required multiple steps to synthesize the template or catalyst in advance of the carbon foam synthesis.

Here, we report a facile one-pot synthesis technique without presynthesis of any templates or catalyst that is able to achieve porous carbon foam with SSA up to 2340 m^2/g. Our approach uses the direct pyrolysis of a sucrose and zinc nitrate mixture, with extremely quick (∼5 min) reaction time and simple postsynthesis treatment. In this method, the zinc nitrate decomposes and generates gas to blow the melted sugar, similar to the role of ammonium salt in Wang's method.[2] The ZnO nanoparticles formed from the decomposition of zinc nitrate can also serve as an etchant during high-temperature annealing[16] to further activate the carbon foam and create more porosity just as in Strubel's method.[3] However, our technique is not just the simple combination of the blowing effect from Wang's method and etching effect in Strubel's method. In our method, the nitrate could also act as an oxidizer to burn the sugar. Meanwhile, the ZnO nanoparticles also act as frames to prevent the collapse of the melted porous sugar during the carbonization process. Both of these factors are critical and make it possible for the reaction to be finished quickly in one step within a few minutes, which, to the best of our knowledge, has not been reported before. Moreover, this technique also offers a way to quickly synthesize other metal or metal oxide/porous carbon composites for multiple applications. In this work, the role of ZnO and annealing temperature on the structure and SSA of the carbon foam were systematically studied. The materials were then evaluated as electrodes for supercapacitors in aqueous electrolyte and showed specific capacitances as high as 280 F/g at a current density of 0.1 A/g, higher than activated carbons and nanocarbons such as carbon nanotubes and graphene.

Received: March 20, 2015
Accepted: April 2, 2015
Published: April 2, 2015

DOI: 10.1021/acsami.5b02453
ACS Appl. Mater. Interfaces 2015, 7, 8952−8960

2. EXPERIMENTAL DETAILS

2.1. Materials Synthesis. The sucrose and $Zn(NO_3)_2{\cdot}6H_2O$ (both from Alfa Aesar) were mixed with different weight ratios. Typically, 1 g of sucrose and 2 g of $Zn(NO_3)_2{\cdot}6H_2O$ (1g:2g; the same naming rule applies for other ratios) were put in a 100 mL beaker and slowly melted and mixed thoroughly to form a uniform viscous mixture using a hot place at 120 °C. Then, the viscous mixture could be quickly carbonized and form carbon foam in about 5 min at ~180 °C on a hot plate or inside a box furnace. If using a hot plate, in order to heat the precursors more uniformly, a heat gun is recommended to heat the side of the beaker and make the entire mixture carbonized. If a box furnace were used, the reaction would be more uniform because the temperature is more uniform. Due to the formation of NO_2 and NO_x gases, it is recommended to place the hot plate or box furnace in a fume hood with good ventilation.

High-temperature annealing experiments were performed by heating the as-prepared carbon foam at 1200 °C in tube furnace under N_2 gas flowing at 150 sccm for 2 h. For some samples, a graphite furnace (GT Thermal Technologies, Inc., Model 1050CG) was used to anneal the samples at up to 2300 °C for 2 h in Ar. In some samples where the annealing temperature was not hot enough to reduce ZnO, the ZnO was etched with HCl, followed by thorough washing with DI water and drying.

2.2. Materials Characterization. Carbon foam samples were characterized using scanning electron microscopy (SEM, Philips XL 30 at 10 kV), transmission electron microscopy (TEM, Phillips CM 200 at 200 kV), thermal gravimetric analysis (TGA, Setaram TG-DTA92), Raman spectroscopy (532 nm, 50 mW excitation laser), and Brunauer–Emmett–Teller (BET) surface area analysis (Micromeritics, Tristar II).

2.3. Electrochemical Measurement. The carbon foam powder was put onto stainless steel discs (1.5 cm diameter) directly without any binder or carbon black to make a ~0.5 mg/cm^2 electrode. For the carbon foams annealed at 1200 °C, to improve the wetting with the electrolyte, we mixed the carbon foam in a slurry with conducting carbon black (10 wt %), polyvinylidene fluoride (PVdF, 10 wt %), and *N*-methyl-2-pyrrolidone (NMP) and coated onto the stainless steel discs as a film. Then, two identical electrodes were assembled into a coin cell with Whatman filter paper as separator and 1 M H_2SO_4 as the electrolyte. The coin cell was sealed with around 1200 psi of pressure. A two-electrode setup was used to measure the performance of the supercapacitors using cyclic voltammetry with a BioLogic VMP3 potentiostat from −0.5 to 0.5 V. The specific capacitance was calculated from the galvanostatic charge–discharge curves using eq 1[17]

$$C = 4I/(m\Delta V/\Delta t) \quad (1)$$

where I is the current used, m is the total mass of carbon foam for both electrodes, and $\Delta V/\Delta t$ was calculated from the slope of the straight part of discharge curve. Electrochemical impedance spectroscopy (EIS) was conducted at open circuit voltage in the frequency range of 1 Hz to 100 kHz with a 5 mV AC amplitude.

3. RESULTS AND DISCUSSION

3.1. Synthesis of Porous Carbon Foam. The synthesis of carbon foam could be achieved through the direct reaction of a sucrose and zinc nitrate mixture in a few minutes (Video S1, Supporting Information). Sucrose and zinc nitrate were first slowly melted and mixed uniformly at a relatively low temperature (~120 °C; Figure 1a). The initiation of the carbonization process was characterized by a color change in the mixture to yellow (Figure 1b) corresponding to the formation of NO_2 from decomposition of $Zn(NO_3)_2$ when the temperature was increased to ~180 °C. The reaction then proceeded according to the general process shown in eq 2, where $Zn(NO_3)_2{\cdot}6H_2O$, a strong oxidizer, decomposed and reacted with sucrose to generate gases (N_2, NO_x, CO_2, etc.),

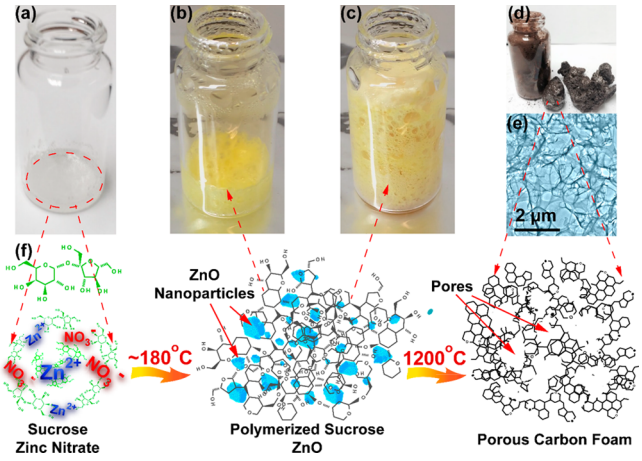

Figure 1. Synthesis process and schematic illustration of carbon foam. (a–e) Different stages of the synthesis process and (f) molecular schematic illustration for the corresponding steps. (a) Starting mixture of sucrose and zinc nitrate precursors (0.5 g of sucrose and 1 g of zinc nitrate shown in the picture); (b and c) the precursors start reacting at ~180 °C, with the zinc nitrate decomposing to ZnO and formation of gases that cause the melted sucrose to blow into a foam-like structure; (d) the carbon foam after further annealing at high temperature; and (e) typical TEM image of carbon foam annealed at 1200 °C.

which acted to blow the melted viscous sugar and cause it to swell (Figure 1b,c).

$$C_{12}H_{22}O_{11} + Zn(NO_3)_2{\cdot}6H_2O \xrightarrow{\sim 180\,^\circ C} C_{foam} + ZnO + N_2\uparrow + H_2O\uparrow + NO_x\uparrow + CO_2\uparrow \quad (2)$$

Meanwhile, the sucrose would dehydrate and polymerize, resulting in the mixture to change to a brown color (abruptly, as shown in Video S1, Supporting Information) and form a foam-like composite containing embedded ZnO nanoparticles (Figure 1f). After the reaction was complete, the ZnO nanoparticles could be removed using acid or through further annealing at high temperatures. ZnO can be reduced by carbon according to eq 3 at 900 °C,[16] and then the resulting zinc can evaporate, leaving the black colored porous carbon foam behind (Figure 1e,f).

$$xC + ZnO \xrightarrow{>900\,^\circ C} (x-1)C + Zn + CO \quad (3)$$

TGA was used to further confirm the reactions. Heating a carbon foam prepared from 1 g of sucrose and 2 g of $Zn(NO_3)_2{\cdot}6H_2O$ (1g:2g carbon foam) in either N_2 or air resulted in the weight loss and differential thermogravimetric curves shown in Figure 2. The weight loss peak at around 250 °C for both samples corresponds to the decomposition of residual $Zn(NO_3)_2{\cdot}6H_2O$. The sample started burning in air and showed a weight loss peak at around 380 °C. For the sample annealed in N_2, the sugar kept carbonizing and showed weight loss until 500 °C. Then, the weight decreased slowly from 500 to 800 °C, which might be caused by the slow reaction between carbon and the ZnO nanoparticles. The weight loss peak around 900 °C should be from the carbothermal reduction of ZnO[16] as described by eq 3.

3.2. the Effect of Precursor Ratio on Morphology and Specific Surface Area of Carbon Foam. Typical SEM images of the carbon foams are show in Figure 3. We can see

DOI: 10.1021/acsami.5b02453
ACS Appl. Mater. Interfaces 2015, 7, 8952–8960

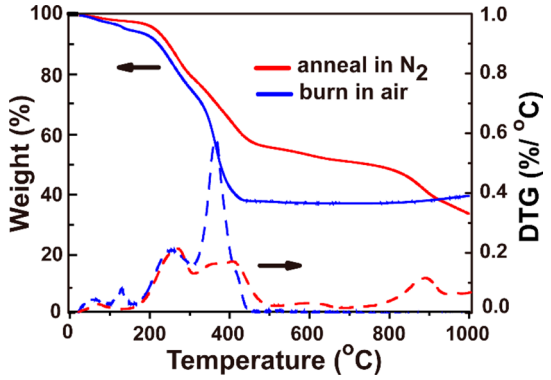

Figure 2. TGA results for 1g:2g carbon foam annealed in (red) N_2 and burning in (blue) air.

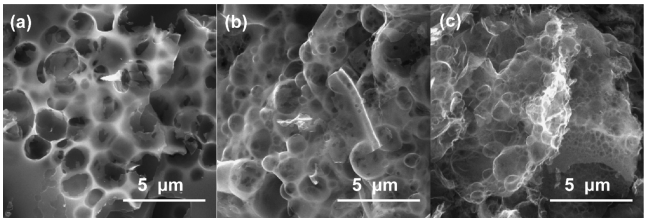

Figure 3. SEM images of carbon foam after annealing at 1200 °C for 2 h made from different sugar to $Zn(NO_3)_2{\cdot}6H_2O$ ratios: (a) 1g:1g, (b) 1g:2g, and (c)1g:3g.

clearly that by increasing the amount of $Zn(NO_3)_2{\cdot}6H_2O$ in the precursor, the carbon foam became more porous and had a greater number of smaller pores. This could be from the increased amount of gas (N_2, NO_x, CO_2, etc.) generated from the decomposition of $Zn(NO_3)_2{\cdot}6H_2O$ and the carbonization of sugar, which could form bubbles in the molten sugar, as seen by the morphology of the carbon foam. Moreover, the additional ZnO nanoparticles can also etch more carbon[16] and form more pores at high temperatures.

To further study the effect of the sugar to $Zn(NO_3)_2{\cdot}6H_2O$ ratio on the SSA of carbon foam, we conducted N_2 adsorption–desorption isotherms measurements on three carbon foam samples with different precursor ratios. Calculated from the curves shown in Figure 4a, the SSAs of the 1g:1g, 1g:2g, 1g:3g carbon foams annealed at 1200 °C for 2 h were around 937, 1690, and 2340 m^2/g, respectively, indicating that the higher the amount of $Zn(NO_3)_2{\cdot}6H_2O$ in the precursor solution, the higher the SSA of the resulting carbon foam. When plotting the SSA against R, where R is the mass of $Zn(NO_3)_2{\cdot}6H_2O$ (g) used to 1 g of sugar, there is a linear relationship. Specifically, we can observe that the SSA increased around 700 m^2/g when the amount of $Zn(NO_3)_2{\cdot}6H_2O$ increased 1 g relative to the amount of sugar. Also, the y-intercept, where $R = 0$, is around 252 m^2/g, which corresponds to the SSA of carbon foam derived from carbonization of pure sucrose without any zinc nitrate, as reported in the literature.[18] This further confirms the contribution of $Zn(NO_3)_2{\cdot}6H_2O$ to increasing the SSA of the carbon foams. As shown in Figure 4a, the 1g:1g carbon foam had a type I isotherm with almost no hysteresis, while the 1g:2g carbon foam starts to show a little hysteresis but still kept the type I shape, indicating its microporous structure. However, the 1g:3g carbon foam showed a type IV isotherm with large hysteresis, which indicates that it contains mesoporosity.[19] The pore size distributions calculated using density function theory (DFT)[20] also showed the pore size changes with increasing $Zn(NO_3)_2{\cdot}6H_2O$ in the precursor (Figure 4b). Specifically, the pore size distributions in the 1g:1g carbon foam are mainly between 2 and 3 nm, while the 1g:2g carbon foam starts having some pore size between 10 and 100 nm. For the 1g:3g carbon foam, however, the mesopores between 5 and 400 nm in size become significant.

These features could be further explained by the TEM images (Figure 5) of the as-made carbon foams that were heated at 350 °C for 30 min. At this point, most of the sugar was carbonized, but ZnO had not been reduced by carbon yet. The carbon adopted a sheet-like morphology and the ZnO nanoparticles could be found interdispersed within. The ZnO nanoparticles in both the 1g:1g and 1g:2g carbon foam mainly had two sizes. The smaller particles with around 5 nm in size were found embedded in the carbon matrix surrounding the bigger particles around 20 nm in size. In the 1g:1g carbon foam (Figure 5a,b), the majority of the ZnO nanoparticles were around 5 nm. However, the bigger particles became significant in the 1g:2g carbon foam (Figure 5c,d). This explains why the 1g:1g carbon foam has a type I isotherm with almost no hysteresis, while the isotherm of the 1g:2g carbon foam starts

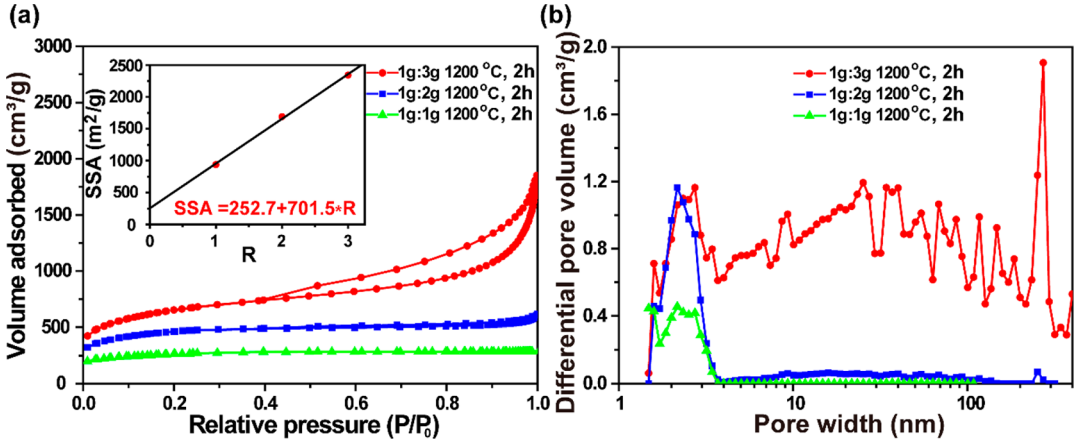

Figure 4. (a) N_2 adsorption–desorption isotherms of carbon foam made from different sugar to $Zn(NO_3)_2{\cdot}6H_2O$ ratio and annealed at 1200 °C for 2 h; (inset) plots the SSA against the grams of $Zn(NO_3)_2{\cdot}6H_2O$ used (R) with 1 g sugar in the precursor; and (b) corresponding pore size distributions calculated using the DFT method.

DOI: 10.1021/acsami.5b02453
ACS Appl. Mater. Interfaces 2015, 7, 8952–8960

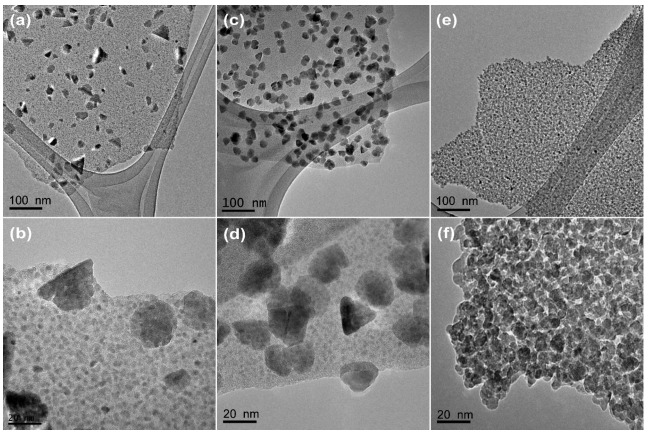

Figure 5. TEM images at different magnifications of carbon foams made from different sugar to $Zn(NO_3)_2{\cdot}6H_2O$ ratios and carbonized at 350 °C for 30 min: (a and b) 1g:1g, (c and d) 1g:2g, and (e and f) 1g:3g.

having the hysteresis feature. The ZnO nanoparticles in the 1g:3g carbon foam are mainly around 10 nm instead of differentiating into two sizes. Moreover, the ZnO nanoparticles are so crowded and interconnecting with each other that the carbon phase no longer looks like a matrix (Figure 5e,f). The aggregation of ZnO nanoparticles makes the 1g:3g carbon foam mesoporous and have a type IV isotherm.

3.3. The Role of ZnO on the Specific Surface Area of Carbon Foam. To study the contribution of ZnO to the SSA at high temperature, we characterized three 1g:2g carbon foam samples treated with different annealing conditions with N_2 adsorption−desorption isotherms. Specifically, after synthesis, all three samples were heated at 600 °C for 2 h, where most of the carbon source changed to carbon but had not reacted with ZnO nanoparticles. For samples S1 and S2, the ZnO was removed with HCl and washed with deionized (DI) water thoroughly. Sample S1 had no further treatment, while S2 was further annealed at 1200 °C. Sample S3 was annealed at 1200 °C directly without removing ZnO beforehand with HCl. Based on the N_2 adsorption−desorption isotherms (Figure 6a), the SSAs of S1 and S2 were 1211 and 1268 m^2/g, respectively, indicating that further annealing at 1200 °C did not change the SSA much once the ZnO was removed. However, the SSA of S3 was 1674 m^2/g, around 400 m^2/g more than that of S1 and S2, revealing that the presence of ZnO can lead to higher SSA after annealing at 1200 °C due to the ability of ZnO to etch carbon. The pore size distribution also reveals that from S1 to S2, further annealing at 1200 °C did not have much change on the amount of micropores but caused a small increase in the mesopore volume. However, the etching effect caused by ZnO nanoparticles at high temperatures makes the differential pore volume peak increase by about one-third in the micropore region.

3.4. The Effect of Annealing on the Specific Surface Area of Carbon Foam. For porous carbon materials, since the annealing temperatures can significantly change the pore volume, bond structures, and surface functional groups, they have a great influence on both the SSA[21−23] and carbon electronic conductivity,[22−26] which are two critical factors for carbon materials in many applications, especially as electrode materials. For this reason, we systematically studied the effect of annealing temperatures on the structure of carbon foam so that good conductivity in the carbon foam could be achieved by annealing the samples at higher temperatures, while still keeping the SSA relatively high. According to the N_2 adsorption−desorption isotherms of 1g:2g carbon foams shown in Figure 7a, when the temperature was increased from 1200 to 1500 °C, the SSA remained almost the same and then started to decrease from 1690 to 1265 m^2/g when the temperature was further increased to 1800 °C. For the sample annealed at 2300 °C, the SSA had only 62 m^2/g remaining.

To understand this decrease in SSA after high-temperature annealing, we used TEM to study the structural changes in the carbon foam. As shown in the TEM images in Figure 8, when the annealing temperature increased, the carbon foam started to crystallize, and its surface became smoother. For the sample annealed at 1200 °C, the surface of the carbon foam sheet was very rough (Figure 8a), while the structure was mostly amorphous, with only one to two layers of graphitic structure (Figure 8b). When the samples were annealed at 1800 °C (Figure 8c,d) and 2300 °C (Figure 8e,f), the surfaces of the foam sheets became smoother, and the structures became more crystalline. The sample annealed at 1800 °C had two to three graphitic layers, while the one annealed at 2300 °C had three or

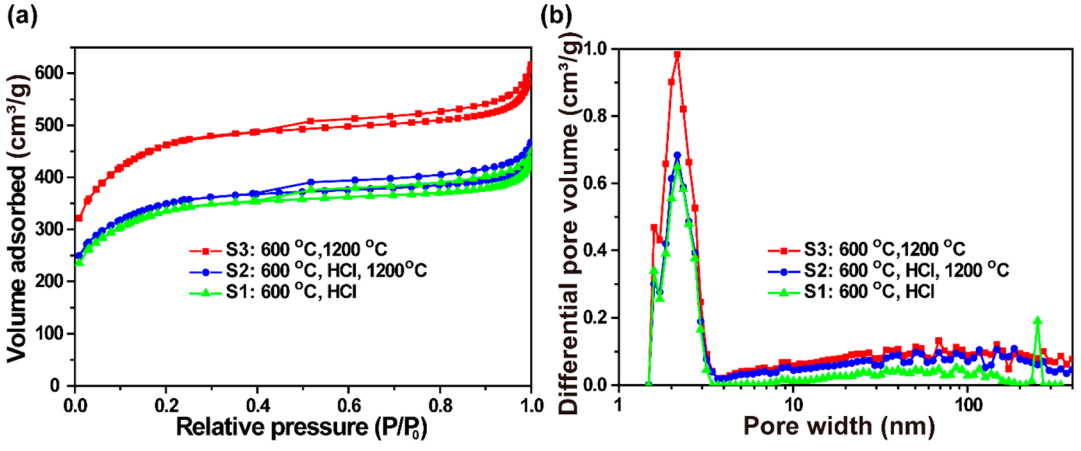

Figure 6. (a) N_2 adsorption−desorption isotherms of 1g:2g carbon foam treated with different conditions. Sample S1 was annealed at 600 °C for 2 h and then treated with HCl to remove ZnO; sample S2 was made from S1 by further annealing at 1200 °C for 2 h; and sample S3 was annealed at 600 °C for 2 h and then further annealed at 1200 °C for 2 h without removing ZnO with HCl. (b) Corresponding pore size distributions calculated using the DFT method.

DOI: 10.1021/acsami.5b02453
ACS Appl. Mater. Interfaces 2015, 7, 8952−8960

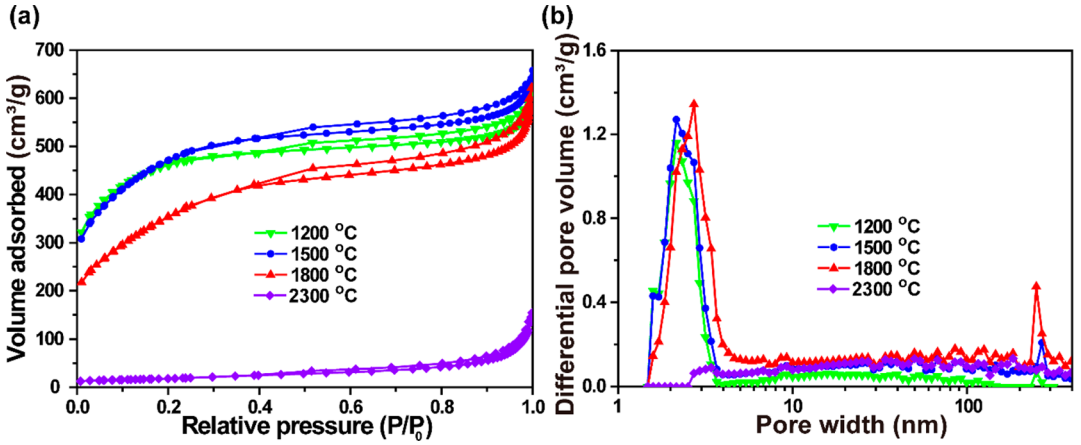

Figure 7. (a) N_2 adsorption–desorption isotherms of the 1g:2g carbon foam annealed at different temperatures: (green) 1200 °C, 2 h; (blue) 1500 °C, 2 h; (red) 1800 °C, 2 h; and (violet) 2300 °C, 2 h. (b) Corresponding pore size distributions calculated using the DFT method.

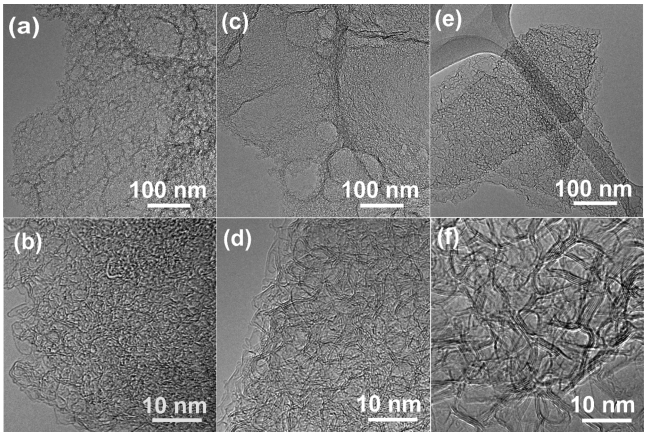

Figure 8. TEM images of carbon foam: (a and b) 1:2 CF annealed at 1200 °C for 2 h, (c and d) 1:2 CF annealed at 1800 °C for 2 h, and (e and f) 1:2 CF annealed at 2300 °C for 2 h.

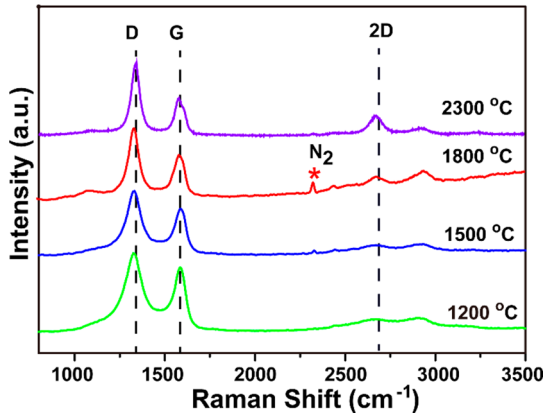

Figure 9. Raman spectra of 1g:2g carbon foam annealed with different temperatures: (green) 1200 °C, 2h; (blue) 1500 °C, 2h; (red) 1800 °C, 2h; and (violet) 2400 °C, 2h. The asterisk (*) denotes N_2 adsorbed from the air during the spectrum acquisition.

more layers. These results indicate that the crystallization process may cause the coalescence or closing of the small pores and lead to the decrease of SSA, which also changes the pore size distribution (Figure 7b). According to Figure 7b, the pores in the microporous region shifted to larger size when the annealing temperatures increased from 1200 to 1800 °C, while the volume of pores in the mesoporous region became higher. When the temperature further reached 2300 °C, the volume of the smallest pores in the microporous region became negligible.

The Raman data shown in Figure 9 also confirm that the carbon foam started to crystallize above 1500 °C, because the 2D band at ~2680 cm^{-1} relating to the stacking order of the graphitic structure along the *c* axis[27] became more significant for samples annealed at 1800 and 2300 °C. Moreover, both the D band at ~1360 cm^{-1} attributed to defect and disorder[28] and the G band at ~1590 cm^{-1} corresponding to the sp^2 carbon network[27,29] became sharper as the annealing temperature increased, which means the high temperature annealing made the carbon more graphitic. Meanwhile, the curvature of the graphitic sheets might introduce more defects, which is consistent with the TEM result (Figure 8 d,f).

3.5. Electrochemical Performance of the Carbon Foams As Supercapacitor Electrodes. To evaluate the electrochemical performance of the carbon foams as the surpercapacitor electrodes, we conducted a two-electrode setup in coin cells in 1 M H_2SO_4 electrolyte. For the batch of carbon foams used for the supercapacitor test, the as-made 1g:3g carbon foams were annealed at 600 °C for 5 h under N_2 atmosphere (designated as 1g:3g 600 °C). Then the ZnO was etched with HCl, followed by washing with DI water and drying at 300 °C. The 1g:3g 700 or 800 °C carbon foams were obtained from the 600 °C foams by further annealing at 700 or 800 °C for 1 h, respectively.

Figure 10a shows the typical cyclic voltammetry (CV) curves of supercapacitors made from 1g:3g 600 °C and Figure 10b shows the galvanostatic charge/discharge curves taken at different current densities. Similar galvanostatic tests were performed on samples with different precursor ratios and annealing temperatures. The specific capacitances of the samples treated with different conditions are shown in Figure 10c–f determined by fitting the slope of the linear part of the discharge curve. The specific capacitance was as high as 280 F/g for the 1g:3g 600 °C carbon foam at a current density of 0.1 A/g, with 207 F/g still remaining even when the current density increased to 10 A/g (Figure 10c).

The other combinations of precursor ratio and annealing temperature showed lower specific capacitances. When the post treatment temperature was held constant (e.g., 600 °C), the specific capacitance increased with the ratio of $Zn(NO_3)_2 \cdot 6H_2O$ in the precursor mixture (Figure 10f), as expected

DOI: 10.1021/acsami.5b02453
ACS Appl. Mater. Interfaces 2015, 7, 8952–8960

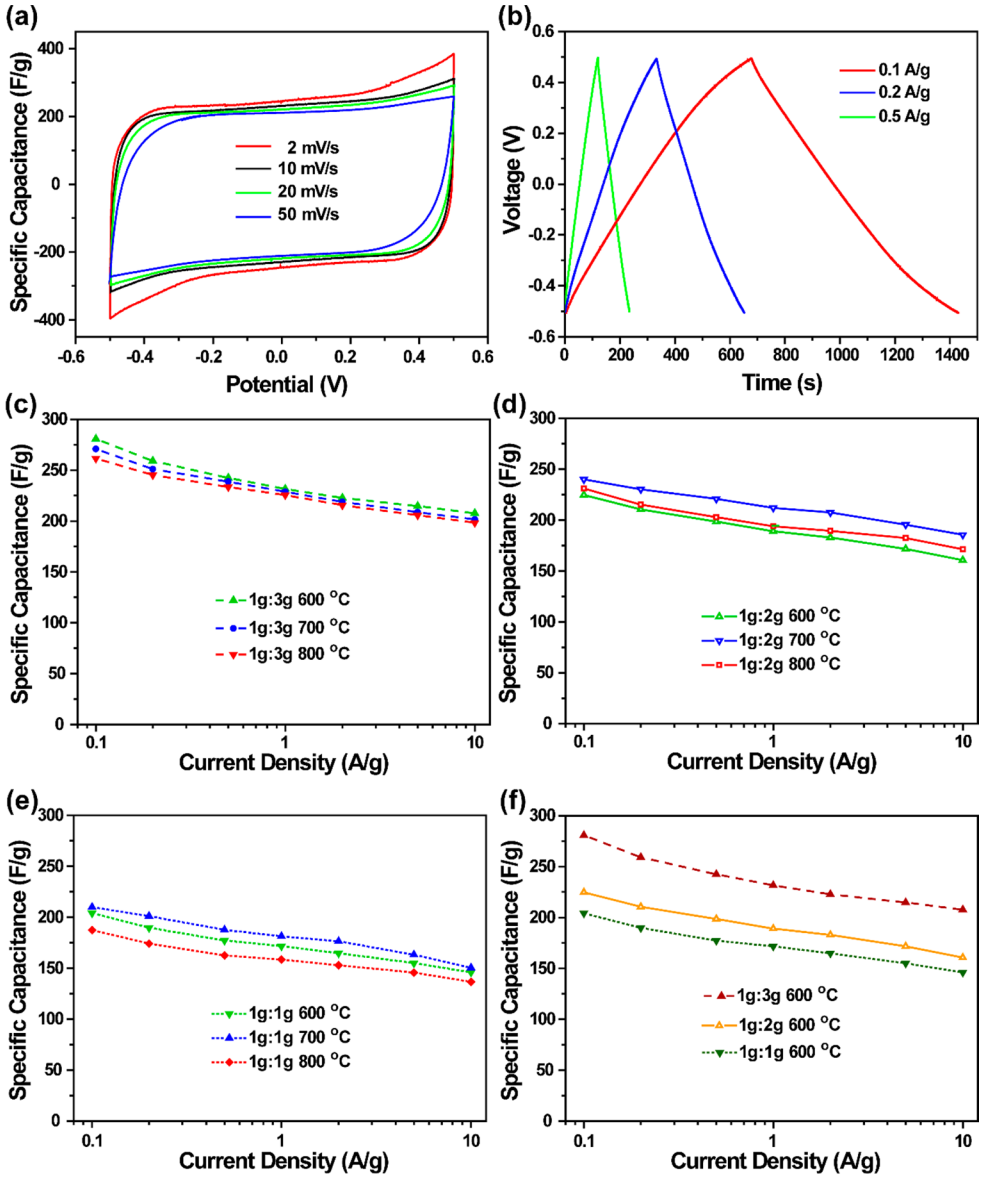

Figure 10. Performance of supercapacitors with carbon foams electrodes in 1 M H_2SO_4 aqueous electrolyte. (a) CV curves obtained at different scan rates for supercapacitors made from 1g:3g 600 °C carbon foam. (b) Galvanostatic charge/discharge curves of supercapacitors made from 1g:3g 600 °C carbon foam at different current densities. The specific capacitances of supercapacitors made from (c) 1g:3g, (d) 1g:2g, and (e) 1g:1g carbon foams treated with different temperatures at different current densities. (f) Specific capacitances of supercapacitors made from 1g:3g, 1g:2g, and 1g:1g carbon foams annealed at 600 °C at different current densities.

because the SSA increased with the ratio of $Zn(NO_3)_2{\cdot}6H_2O$. Calculated from the N_2 adsorption−desorption isotherms shown in Figure S1a (Supporting Information), the SSAs for 1g:1g, 1g:2g, and 1g:3g carbon foams annealed at 600 °C were 788, 1069, and 1731 m^2/g, respectively. Although the SSAs were lower than those of corresponding carbon foams annealed at 1200 °C with ZnO nanoparticles, the shape of the N_2 adsorption−desorption isotherms and the pore size distribution curves were similar to those shown in Figure 4.

According to previous studies, the annealing temperature has an influence on the carbon surface functional groups, especially oxygenated groups,[22−26,30] which directly relate to the wettability of the carbon surface with the electrolyte. With the removal of oxygenated surface groups at higher temperatures, the carbon is expected to have less wettability with the aqueous electrolyte. The annealing temperature also affects the carbon conductivity dramatically, especially in the range of 600−800 °C,[22−25] where the conductivity can increase 1 order of magnitude or more. This change could also be seen from the EIS measurement in Figure 11. In the Nyquist plots, the intercept with the real axis at high frequency represents the ohmic resistance, including the resistance of the electrode materials, electrolyte, and the contact resistance. The ohmic resistance was similar for all of the different samples. Among each batch of carbon foam prepared with the same precursor ratio, the charge transfer resistance R_{ct}, represented by the semicircle regions, decreased when the annealing temperature increased, especially from 600 to 700 °C. Specifically, the 1g:3g carbon foams (Figure 11a) have much larger resistance than the 1g:1g (Figure 11c) and 1g:2g (Figure 11d) carbon foams at different temperatures. Figure 11b compares the Nyquist plots for the carbon foams with different precursor ratios annealed at 600 °C. Because the 1g:3g carbon foams are more porous and have more large pores (Figure S1b, Supporting Information),

DOI: 10.1021/acsami.5b02453
ACS Appl. Mater. Interfaces 2015, 7, 8952−8960

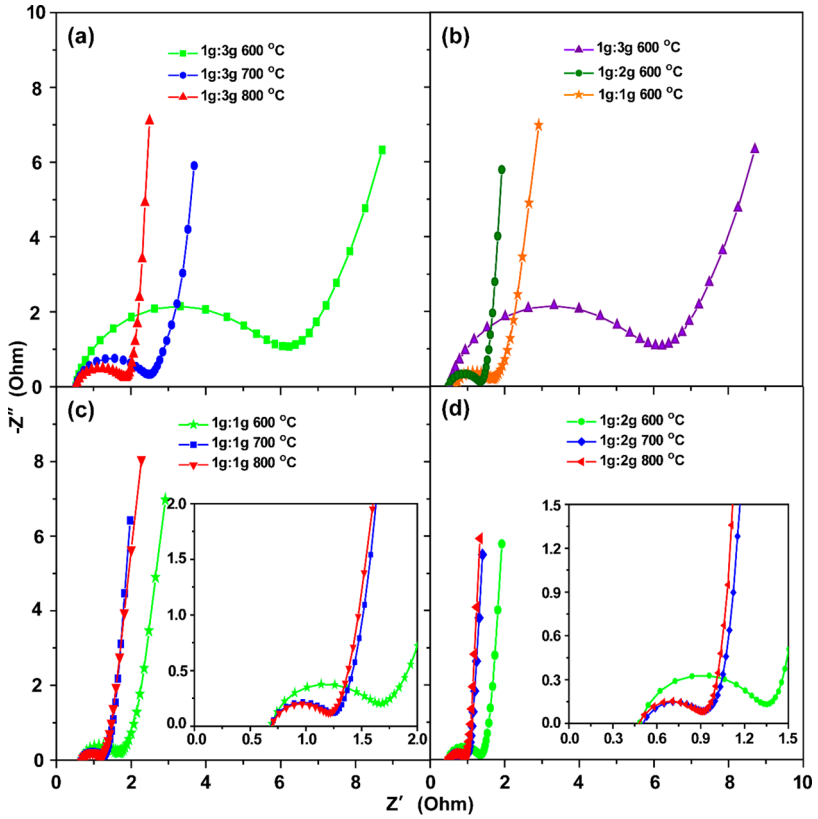

Figure 11. EIS measurement of supercapacitors made of different carbon foams annealed with different temperatures: (a) 1g:3g carbon foams, (b) carbon foams with different precursor ratio annealed at 600 °C, (c) 1g:1g and (d) 1g:2g carbon foams; (c and d, insets) magnified view of the high-frequency region.

the contact resistance between the carbon foam particles is more significant than that of the less porous 1g:2g and 1g:1g carbon foams. The difference in the pore structure as a result of the three carbon foam precursor ratios also causes the change of carbon conductivity to have a different influence on the capacitance performance when combined with other factors, as we discuss below. Considering that these two factors can affect the capacitance properties of the carbon, the performance of the supercapacitors made from all three types of carbon foams treated with three different temperatures (600, 700, and 800 °C) was studied and shown in Figure 10c–e.

As Figure 10c shows, the specific capacitances of the 1g:3g carbon foams kept decreasing when the annealing temperature increased from 600 to 800 °C, despite the fact that the carbon conductivity has increased (Figure 11a). Because the ultrahigh SSA (1731 m^2/g, Figure S1a, Supporting Information) and mesoporous structure (Figure S1b, Supporting Information) indicate a high contact area with the electrolyte, this shows that temperature-dependent changes on the interfacial properties of the carbon foam (e.g., wettability) outweigh the effect of changes on the carbon conductivity. However, for both 1g:1g and 1g:2g carbon foams, because the SSAs are much lower than that of 1g:3g carbon foam and the pores are mainly micropores, the maximum specific capacitance obtained at 700 °C should be due to the significant increase of the carbon conductivity[22−25] (Figure 11c,d) and the increase in the pore sizes (Figures 6b and 7b). The specific capacitances started decreasing at 800 °C (Figure 10d,e), even though the conductivity was slightly better than that of the carbon foam annealed at 700 °C (Figure 11c,d). This could be due to the surface dewetting from to the loss of the oxygenated goups.[22,24,25] A similar phenomenon showing a dependence of the specific capacitance on the annealing temperature was also reported on other porous carbons recently.[1]

The supercapacitor made with 1g:2g 700 °C carbon foam was used to study the cycle performance. The capacitance retention remained at 100% (Figure S2, Supporting Information) after 10 000 charge/discharge cycles at a current density of 10 A/g, which demonstrates very good long-term stability.

To further study the influence of the wettability of the carbon foam surface on the specific capacitance, a 1g:2g carbon foam annealed at 1200 °C with ZnO nanoparticles for 2 h was used to test the performance as supercapacitor electrodes. Due to the etching effect of ZnO nanoparticles at high temperature, the SSA was as high as 1690 m^2/g (Figure 7a), much higher than that of 1g:2g 600 °C carbon foam, 1069 m^2/g (Figure S1a, Supporting Information). Moreover, the carbon conductivity also improved a lot, as seen by the rectangular shape of the CV curves (Figure S3a, Supporting Information). However, due to the bad wettability, the capacitance was not as good as expected. The specific capacitance was only around 125 F/g at a 50 mV/s scan rate, while the one for the 1g:2g 600 °C carbon foam was as high as around 175 F/g at same scan rate (Figure S3b, Supporting Information). The results reveal that in aqueous electrolyte, the wettability could be the dominant factor on the performance of the carbon foam-based supercapacitors.

From these results, we see that the carbon foams can act as high-capacitance supercapacitor electrodes, with a specific capacitance as high as 280 F/g at a current density of 0.1 A/g, which is higher than most values reported for carbon nanotubes (50−100 F/g),[31] graphene (100−250 F/g),[32,33] and

DOI: 10.1021/acsami.5b02453
ACS Appl. Mater. Interfaces 2015, 7, 8952−8960

activated carbon (100−200 F/g).[10,31,34] The carbon foam performance is comparable with the recently demonstrated three-dimensional strutted graphene (250 F/g, at 0.5 A/g),[2] KOH activated porous carbon nanosheets (300 F/g, at 0.5 A/g),[35] and even nitrogen doped KOH activated porous carbon (300 F/g, at 0.1 A/g).[36] However, the synthesis method used to achieve our highly porous carbon foam is simple and does not require doping or presynthesized templates or particles.

4. CONCLUSIONS

In summary, we have developed a facile one-pot technique able to fabricate foam-like porous carbon without presynthesizing any hard templates or precursors. By simply adjusting the ratio of sugar to $Zn(NO_3)_2 \cdot 6H_2O$, the carbon foams with different SSAs and pore size distribution can be easily achieved at a large scale. Due to the unique roles that ZnO nanoparticles act during the synthesis and post annealing stages, a high SSA up to 2340 m^2/g is obtained. The excellent electrochemical performance of the carbon foam makes it very promising for potential applications as electrode materials in the energy storage field. Moreover, the unique properties and the scalable synthesis make these novel carbon foams suitable for many other applications, such as sorbents and catalyst supports.

■ ASSOCIATED CONTENT

Supporting Information

Video of real-time synthesis of carbon foam, BET data of carbon foam prepared at 600 °C, cycle life of supercapacitor made with 1g:2g carbon foam prepared at 700 °C. This material is available free of charge via the Internet at http://pubs.acs.org.

■ AUTHOR INFORMATION

Corresponding Author

*E-mail: Candace.chan@asu.edu.

Notes

The authors declare no competing financial interest.

■ ACKNOWLEDGMENTS

This research was supported using new faculty startup funds from the Fulton Schools of Engineering at ASU. The authors gratefully acknowledge the use of facilities within the LeRoy Eyring Center for Solid State Science, the Goldwater Environmental Laboratory at Arizona State University. We would also like to thank Y. Li and Q. Cheng for assistance with the electrochemical measurements. We would like to thank D. Wright for assistance with the high-temperature annealing measurements and C. Guo for assistance with the Raman measurements.

■ REFERENCES

(1) Sevilla, M.; Fuertes, A. B. Direct Synthesis of Highly Porous Interconnected Carbon Nanosheets and Their Application as High-Performance Supercapacitors. *ACS Nano* **2014**, *8*, 5069−5078.

(2) Wang, X.; Zhang, Y.; Zhi, C.; Wang, X.; Tang, D.; Xu, Y.; Weng, Q.; Jiang, X.; Mitome, M.; Golberg, D.; et al. Three-Dimensional Strutted Graphene Grown by Substrate-Free Sugar Blowing for High-Power-Density Supercapacitors. *Nat. Commun.* **2013**, *4*, 2905.

(3) Strubel, P.; Thieme, S.; Biemelt, T.; Helmer, A.; Oschatz, M.; Brückner, J.; Althues, H.; Kaskel, S. ZnO Hard Templating for Synthesis of Hierarchical Porous Carbons with Tailored Porosity and High Performance in Lithium-Sulfur Battery. *Adv. Funct. Mater.* **2015**, *25*, 287−297.

(4) Hata, K.; Futaba, D. N.; Mizuno, K.; Namai, T.; Yumura, M.; Iijima, S. Water-Assisted Highly Efficient Synthesis of Impurity-Free Single-Walled Carbon Nanotubes. *Science* **2004**, *306*, 1362−1364.

(5) Ren, Z. F.; Huang, Z. P.; Xu, J. W.; Wang, J. H.; Bush, P.; Siegal, M. P.; Provencio, P. N. Synthesis of Large Arrays of Well-Aligned Carbon Nanotubes on Glass. *Science* **1998**, *282*, 1105−1107.

(6) Reina, A.; Jia, X.; Ho, J.; Nezich, D.; Son, H.; Bulovic, V.; Dresselhaus, M. S.; Kong, J. Large Area, Few-Layer Graphene Films on Arbitrary Substrates by Chemical Vapor Deposition. *Nano Lett.* **2009**, *9*, 30−35.

(7) Kim, K. S.; Zhao, Y.; Jang, H.; Lee, S. Y.; Kim, J. M.; Kim, K. S.; Ahn, J.-H.; Kim, P.; Choi, J.-Y.; Hong, B. H. Large-Scale Pattern Growth of Graphene Films for Stretchable Transparent Electrodes. *Nature* **2009**, *457*, 706−710.

(8) Marcano, D. C.; Kosynkin, D. V.; Berlin, J. M.; Sinitskii, A.; Sun, Z.; Slesarev, A.; Alemany, L. B.; Lu, W.; Tour, J. M. Improved Synthesis of Graphene Oxide. *ACS Nano* **2010**, *4*, 4806−4814.

(9) Liang, Y. T.; Hersam, M. C. Highly Concentrated Graphene Solutions via Polymer Enhanced Solvent Exfoliation and Iterative Solvent Exchange. *J. Am. Chem. Soc.* **2010**, *132*, 17661−17663.

(10) Fang, B.; Binder, L. A Modified Activated Carbon Aerogel for High-Energy Storage in Electric Double Layer Capacitors. *J. Power Sources* **2006**, *163*, 616−622.

(11) Lukens, W. W.; Stucky, G. D. Synthesis of Mesoporous Carbon Foams Templated by Organic Colloids. *Chem. Mater.* **2002**, *14*, 1665−1670.

(12) Al-Muhtaseb, S. A.; Ritter, J. A. Preparation and Properties of Resorcinol-Formaldehyde Organic and Carbon Gels. *Adv. Mater.* **2003**, *15*, 101−114.

(13) Fechler, N.; Wohlgemuth, S.-A.; Jäker, P.; Antonietti, M. Salt and Sugar: Direct Synthesis of High Surface Area Carbon Materials at Low Temperatures via Hydrothermal Carbonization of Glucose under Hypersaline Conditions. *J. Mater. Chem. A* **2013**, *1*, 9418.

(14) Wei, L.; Nitta, N.; Yushin, G. Lithographically Patterned Thin Activated Carbon Films as a New Technology Platform for On-Chip Devices. *ACS Nano* **2013**, *7*, 6498−6506.

(15) Wang, D.-W.; Li, F.; Liu, M.; Lu, G. Q.; Cheng, H.-M. 3D Aperiodic Hierarchical Porous Graphitic Carbon Material for High-Rate Electrochemical Capacitive Energy Storage. *Angew. Chem., Int. Ed. Engl.* **2008**, *47*, 373−376.

(16) Chen, H.-K. Kinetic Study on the Carbothermic Reduction of Zinc Oxide. *Scand. J. Metall.* **2001**, *30*, 292−296.

(17) Stoller, M. D.; Ruoff, R. S. Best Practice Methods for Determining an Electrode Material's Performance for Ultracapacitors. *Energy Environ. Sci.* **2010**, *3*, 1294−1301.

(18) Armandi, M.; Bonelli, B.; Geobaldo, F.; Garrone, E. Nanoporous Carbon Materials Obtained by Sucrose Carbonization in the Presence of KOH. *Microporous Mesoporous Mater.* **2010**, *132*, 414−420.

(19) Sing, K. S. W.; Everett, D. H.; Haul, R. A. W.; Moscou, L.; Pierotti, R. A.; Rouquérol, J.; Siemieniewska, T. Reporting Physisorption Data for Gas/Solid Systems with Special Reference to the Determination of Surface Area and Porosity (Recommendations 1984). *Pure Appl. Chem.* **1985**, *57*, 603−619.

(20) Ravikovitch, P. I.; Neimark, A. V. Characterization of Nanoporous Materials from Adsorption and Desorption Isotherms. *Colloids Surfaces A Physicochem. Eng. Asp.* **2001**, *187*−*188*, 11−21.

(21) Liu, B.; Shioyama, H.; Jiang, H.; Zhang, X.; Xu, Q. Metal-Organic Framework (MOF) as a Template for Syntheses of Nanoporous Carbons as Electrode Materials for Supercapacitor. *Carbon* **2010**, *48*, 456−463.

(22) Ruiz, V.; Blanco, C.; Raymundo-Piñero, E.; Khomenko, V.; Béguin, F.; Santamaría, R. Effects of Thermal Treatment of Activated Carbon on the Electrochemical Behaviour in Supercapacitors. *Electrochim. Acta* **2007**, *52*, 4969−4973.

(23) Adinaveen, T.; Kennedy, L. J.; Vijaya, J. J.; Sekaran, G. Surface and Porous Characterization of Activated Carbon Prepared from Pyrolysis of Biomass (Rice Straw) by Two-Stage Procedure and Its Applications in Supercapacitor Electrodes. *J. Mater. Cycles Waste Manag.* **2014**, DOI: 10.1007/s10163-014-0302-6.

DOI: 10.1021/acsami.5b02453
ACS Appl. Mater. Interfaces 2015, 7, 8952−8960

(24) Sánchez-González, J.; Stoeckli, F.; Centeno, T. A. The Role of the Electric Conductivity of Carbons in the Electrochemical Capacitor Performance. *J. Electroanal. Chem.* **2011**, *657*, 176−180.
(25) Pandolfo, A. G.; Hollenkamp, A. F. Carbon Properties and Their Role in Supercapacitors. *J. Power Sources* **2006**, *157*, 11−27.
(26) Kennedy, L. J.; Vijaya, J. J.; Sekaran, G. Electrical Conductivity Study of Porous Carbon Composite Derived from Rice Husk. *Mater. Chem. Phys.* **2005**, *91*, 471−476.
(27) Pimenta, M. A.; Dresselhaus, G.; Dresselhaus, M. S.; Cançado, L. G.; Jorio, A.; Saito, R. Studying Disorder in Graphite-Based Systems by Raman Spectroscopy. *Phys. Chem. Chem. Phys.* **2007**, *9*, 1276−1291.
(28) Jawhari, T.; Roid, A.; Casado, J. Raman Spectroscopic Characterization of Some Commercially Available Carbon Black Materials. *Carbon* **1995**, *33*, 1561−1565.
(29) Malard, L. M.; Pimenta, M. A.; Dresselhaus, G.; Dresselhaus, M. S. Raman Spectroscopy in Graphene. *Phys. Rep.* **2009**, *473*, 51−87.
(30) Darmstadt, H.; Roy, C.; Kaliaguine, S.; Choi, S. .; Ryoo, R. Surface Chemistry of Ordered Mesoporous Carbons. *Carbon* **2002**, *40*, 2673−2683.
(31) Zhang, L. L.; Zhao, X. S. Carbon-Based Materials as Supercapacitor Electrodes. *Chem. Soc. Rev.* **2009**, *38*, 2520−2531.
(32) Luo, J.; Jang, H. D.; Huang, J. Effect of Sheet Morphology on the Scalability of Graphene-Based Ultracapacitors. *ACS Nano* **2013**, *7*, 1464−1471.
(33) Yoo, J. J.; Balakrishnan, K.; Huang, J.; Meunier, V.; Sumpter, B. G.; Srivastava, A.; Conway, M.; Reddy, A. L. M.; Yu, J.; Vajtai, R.; et al. Ultrathin Planar Graphene Supercapacitors. *Nano Lett.* **2011**, *11*, 1423−1427.
(34) Xing, W.; Huang, C. C.; Zhuo, S. P.; Yuan, X.; Wang, G. Q.; Hulicova-Jurcakova, D.; Yan, Z. F.; Lu, G. Q. Hierarchical Porous Carbons with High Performance for Supercapacitor Electrodes. *Carbon* **2009**, *47*, 1715−1722.
(35) Fan, X.; Yu, C.; Yang, J.; Ling, Z.; Hu, C.; Zhang, M.; Qiu, J. A Layered-Nanospace-Confinement Strategy for the Synthesis of Two-Dimensional Porous Carbon Nanosheets for High-Rate Performance Supercapacitors. *Adv. Energy Mater.* **2014**, DOI: 10.1002/aenm.201401761.
(36) Zhao, L.; Fan, L.-Z.; Zhou, M.-Q.; Guan, H.; Qiao, S.; Antonietti, M.; Titirici, M.-M. Nitrogen-Containing Hydrothermal Carbons with Superior Performance in Supercapacitors. *Adv. Mater.* **2010**, *22*, 5202−5206.

DOI: 10.1021/acsami.5b02453
ACS Appl. Mater. Interfaces 2015, 7, 8952−8960